Genetic and epigenetic characterization of growth hormone - secreting pituitary tumors

Niko Välimäki,[1,2] Camilla Schalin-Jäntti,[3] Atte Karppinen,[4] Anders Paetau,[5] Leena Kivipelto,[4] Lauri A Aaltonen,[1,2] Auli Karhu[1,2*]

[1]Department of Medical and Clinical Genetics, University of Helsinki, 00014 Helsinki, Finland

[2]Applied Tumor Genomics, Research Programs Unit, FI-00014 University of Helsinki, Finland

[3]Endocrinology, Abdominal Center, University of Helsinki and Helsinki University Hospital, 00029 Helsinki, Finland

[4]Department of Neurosurgery, University of Helsinki and Helsinki University Hospital, 00029 Helsinki, Finland

[5]Department of Pathology, HUSLAB, University of Helsinki, 00014 Helsinki, Finland

Running title: Genetic and epigenetic characterization of somatotropinomas

Key words: Pituitary tumor, Somatic landscape, Aneuploidy, DNA methylation, Tumor subtypes

Financial support: This work was supported by grants from the Academy of Finland's Center of Excellence Program 2012–2017 (#250345) and 2018–2025 (#31204) (LAA, AK), the Academy of Finland (#287665) (NV), and the Finnish Cancer Society (160081) (AK), the Helsinki University Hospital Research Funds (TYH2017138 and TYH2018223) (CSJ) and Finska Läkaresällskapet (CSJ).

Corresponding author: Auli Karhu, Biomedicum Helsinki, Research Programs Unit, PO Box 63 (Haartmaninkatu 8), 00014 University of Helsinki, Tel: +358 2 94125612, E-mail: auli.karhu@helsinki.fi

Conflict of Interest Disclosure: The authors declare no potential conflicts of interest

Abstract

Somatic driver mechanisms of pituitary adenoma pathogenesis have remained incompletely characterized and apart from mutations in the stimulatory Gα protein ($G\alpha_s$ encoded by *GNAS*) resulting activated cAMP synthesis, pathogenic variants are rarely found in growth hormone-secreting pituitary tumors (somatotropinomas).

The purpose of the current work was to clarify how genetic and epigenetic alterations contribute to the development of somatotropinomas by conducting an integrated copy-number alteration, whole-genome- and bisulfite sequencing, and transcriptome analysis of 21 tumors. Somatic mutation burden was low but somatotropinomas formed two subtypes associated with distinct aneuploidy rates and unique transcription profiles. Tumors with recurrent chromosome aneuploidy (CA) were *GNAS* mutation negative (*Gsp*-). The chromosome stable (CS) –group contained *Gsp*+ somatotropinomas and two totally aneuploidy-free *Gsp*- tumors. Genes related to the mitotic G1/S-checkpoint transition, were differentially expressed in CA- and CS-tumors indicating difference in mitotic progression. Also pituitary tumor transforming gene 1 (PTTG1), a regulator of sister chromatid segregation, showed abundant expression in CA-tumors. Moreover, somatotropinomas displayed distinct *Gsp* genotype-specific methylation profiles. Expression quantitative methylation (eQTM) analysis revealed that inhibitory Gα ($G\alpha_i$) –signaling is activated in *Gsp*+ tumors.

These findings suggest that in *Gsp*- somatotropinomas aneuploidy through modulated driver pathways may be a causative mechanism for tumorigenesis, whereas *Gsp*+ tumors in response to mitogenic cAMP-signaling caused by *GNAS* mutation are characterized by DNA methylation activated $G\alpha_i$ –signaling.

Significance: These findings provide valuable new information about subtype-specific pituitary tumorigenesis and may help to elucidate the mechanisms of aneuploidy also in other tumor types.

Introduction

Pituitary adenomas are common and comprise 15% of all diagnosed intracranial neoplasms. The overall rate of pituitary tumors in the general population is one case in 1064 [1]. The most common functioning pituitary tumors hypersecrete prolactin (PRL) (40%). Growth hormone (GH) –secreting adenomas (somatotropinomas) constitute 15-20%, and usually lead to increased height (gigantism) in children or adolescents. In adults, hypersecretion of GH causes acromegaly, and leads to overgrowth of bone and cartilage, insulin resistance, hypertension, cardiovascular and respiratory complications, and increased risk of neoplasms. Despite being benign, excess GH production is associated with increased morbidity and reduced life expectancy [2, 3, 4].

The majority of pituitary adenomas arise in a sporadic setting and are considered to be unicellular in origin. As in other neoplasms, pituitary tumor formation and dysregulated hormone secretion are results of series of genetic and epigenetic alterations upsetting the balance between proliferation and apoptosis. The most frequently described somatic pathogenic events occurring in somatotropinomas are gain-of-function mutations in the *stimulatory guanine nucleotide (GTP) binding protein alpha* ($G\alpha_s$) encoded by the *GNAS* gene. This G*sp* oncogene contributes to constitutive synthesis of cyclic adenosine monophosphate (cAMP), activation of protein kinase A (PKA) pathway, and subsequent tumor formation. *Gsp* mutations occur in ~35% of somatotropinomas [5, 6]. Next generation sequencing has shown that the somatic background of pituitary adenomas is calm and single nucleotide- (SNV) and structural variants (SV) are rarely found. Therefore, the exact mechanisms of tumorigenesis often remain unknown [7, 8, 9, 10, 11, 12].

Numerical alterations of whole chromosomes, aneuploidy, is observed in a subset of pituitary tumors [8, 12]. Aneuploidy is frequently noted in solid and malignant tumors and is often associated with tumor recurrence and drug resistance in some tumor types [13, 14]. Shuffling of genomic content through aneuploidy facilitates loss of heterozygosity (LOH) of tumor suppressors and increases copy number of oncogenes and can constitute a powerful driver for tumor progression. In addition, epigenetic modifications associated to changes in gene expression are considered potential causes of pituitary tumor initiation and development [15].

Apart from the *Gsp*+ driver mutation, mechanisms of pituitary adenoma pathogenesis have remained incompletely characterized, and improved understanding of uncontrolled cell growth associated with pituitary tumors is required. The purpose of the current work was to clarify how somatic alterations drive development of somatotropinomas and discover subgroup-specific somatic patterns. This was done by dissecting

associations between somatic copy number alterations (SCNA), gene expression and DNA methylation in *GNAS* mutation negative (*Gsp*-) and positive (*Gsp*+) pituitary tumors. In addition, whole genome sequencing (WGS) was performed to identify somatic SNV and SV changes.

Here we found that somatotropinomas form two tumor subtypes associated with distinct aneuploidy rates and transcription profiles. Our results indicate that defective chromosomal segregation may underlie the development of aneuploidy and tumor initiation in a subset of *Gsp*- somatotropinomas. Further, we show that *Gsp* mutation status is the major determinant of methylation profiles of somatotropinomas, and that methylation regulated transcription activates an adaptive response to elevated cAMP levels in *Gsp*+ tumors.

Material and Methods

Patient material

We studied somatotropinomas from twenty one patients (13 males and 8 females, mean age at diagnosis 43 years [range 14-69 years]) (Table 1). The tumor samples were collected between 2009 and 2015 at the Helsinki University Hospital and frozen while fresh. The study was approved by the Ethics Committee of the Hospital district of Helsinki (Dnr. 408/13/03/03/2009). All patients had given informed consent for sample collection and analysis. In the case of minor, a parent gave the consent. All research conformed with the principles of the Declaration of Helsinki. The tumor percentages (>95%) were verified with hematoxylin and eosin stainings. All patients were mutation negative for the established germline mutations associated with pituitary neoplasia (Supplementary Methods). Seven tumors were *Gsp*+ and 14 tumors *Gsp*-. Seven patients have hormonally active disease and are treated with post-operative somatostatin analogue therapy (ST3, ST6, ST13, ST16, ST17, ST19, ST21), one (ST6) of them is on somatostatin-cabergoline combination therapy and two (ST3, ST17) on somatostatin-pegvisomant combination therapy. Currently, 14 patients are in hormonal remission, while three non-compliant patients (ST3, ST7, ST22) are not, and current medical therapy of four patients (ST2, ST8, ST14, ST15) is not known (Table 1).

WGS, SCNA and gene expression profiling

Genomic DNA was extracted by FastDNA Spin Kit (MP Biomedicals) (tumors) and DNeasy Blood and Tissue Kit (Qiagen) (blood). The *AIP* and *Gsp* mutation status was identified by capillary sequencing as described earlier [6]. The WGS genomic DNA libraries were prepared according to Illumina PE sequencing protocols

and sequenced to at least 40x median coverage on the Illumina HiSeq 2000 platform (2x100bp PE) (Beijing Genomics Institute, BGI Tech Solutions Co., Ltd., China). A genome-wide analysis of tumors for somatic SNVs and SVs was performed as described previously [8]. The somatic variants in tumors ST2-12 were identified by filtering against a patient-matched blood sample. For the *Gsp*- tumors ST13, ST16, ST18-ST20 and ST22, patient-matched germline variants were not available, and somatic variants were identified by filtering against all variants in gnomAD (r2.0.1) (https://gnomad.broadinstitute.org), 1000 genomes project (phase 3, 20130502) (http://www.internationalgenome.org/home), Sequencing Initiative Suomi (SISu, accessed on March 2016) (http://www.sisuproject.fi/) and an in-house collection of 339 normal tissue WGS samples. The remaining variants were filtered to a minimum coverage of 10 reads, minimum alternative allele coverage of six, and minimum quality score of 40 (phred-scale).

SCNA analysis was performed using SNP arrays (1kGP HumanOmni2.5-8 BeadChip, Illumina, Inc.). Analysis was performed as described previously [8] comparing individuals' tumor sample to its corresponding normal blood derived DNA using Genomics Suite v.6.5 (Partek) with a GC-wave correction. Genomic instability percentage (GI%) was determined by dividing the number of altered chromosomal arms in the tumor by the total number of chromosomal arms.

RNA was extracted with RNeasy Mini Kit (Qiagen). Expression profiles were generated using GeneChip™ Human Transcriptome Array 2.0 array (Thermo Fisher Scientific). cDNA synthesis, labeling, and hybridization was performed according to the manufacturer's instructions. Quality control, normalization, and analysis of data were carried out using Transcriptome Analysis Console v 3.0 (Thermo Fisher Scientific). Unsupervised hierarchical clustering of 1000 probes with the largest variance was done using cosine distance with bottom-up average linking. The annotation file HTA-2_0.na35.2.hg19.transcript and ANOVA were used to determine differentially expressed genes between tumor groups. Differentially expressed genes were filtered using false discovery rate (FDR)< 5% and fold change $|FC| > 2$.

Bisulfite sequencing and data processing

The target region bisulfite sequencing (TBS) of somatotropinomas was performed utilizing the SureSelectXT Human Methyl. Seq (Agilent Technologies, Inc.) target enrichment system. Illumina paired-end sequencing for libraries was done using 126 base-pair read length and the HiSeq2500 platform (Illumina, Inc.) (Beijing Genomics Institute, BGI Tech Solutions Co., Ltd.).

The raw TBS data were preprocessed with the bismark (v0.16.3) pipeline, bowtie2 (v2.3.0) and the human reference genome (UCSC hg19). A total of 8,493,667 CpGs were observed with a minimum coverage of two, out of which 4,527,285 CpGs passed the minimum coverage in at least four tumors. CpG methylation levels were quantified using bsseq (v1.10.0) and DSS (v2.14.0) as follows. An unsupervised, genome-wide analysis was done using bsseq quantification of the CpG methylation levels: the TBS target regions (N=350,539) were filtered to a minimum of three CpGs that passed minimum coverage (N=198,649). The default bsseq smoothing was applied to quantify the methylation level of each target region. An unsupervised hierarchical clustering of 50 000 TBS regions with the largest variance was done using cosine distance with bottom-up average linking. Supervised analysis of differentially methylated regions (DMRs) used the default DSS smoothing to test for a minimum mean methylation difference of 0.2 in a two-group comparison. The DMRs were filtered with the default DSS settings (a minimum of 3 CpGs, minimum 50 bps and $P<10^{-5}$).

The gene annotation and their genomic coordinates were based on Ensemble (v82, hg19). The promoter regions were defined as going from −1kb to +2kb relative to the transcription starting site (TSS), gene bodies (+2kb, relative to the TSS, to the end of the gene). Other genomic annotations were downloaded from the UCSC table browser (accessed on August 2017) for ENCODE enhancer regions (6 human cell lines; awg segmentation combined), DNaseI Hypersensitivity Clusters (ENCODE v3), ENCODE transcription factor clusters (TFBS clusters v3; 161 factors) including the CCCTC-binding factor (CTCF) sites, and CpG islands [16]. CpG island shores were composed of 2kb upstream and downstream regions flanking the CpG islands. Methylation differences with regards to replication timing were annotated based on HeLa cell line data [17].

CpG methylation levels were quantified within [0, 1], where 0 and 1 correspond to total absence and presence of the mark respectively.

Expression quantitative methylation (eQTM) analysis

eQTM analysis was used to identify association between methylation and gene expression levels. The DMRs and their nearby genes were tested for association, also known as cis-eQTM [18], using MatrixEQTL (v2.1.1). The cis-eQTMs were filtered to a maximum 20 Kbp distance between the gene and DMR. The resulting associations were filtered to FDR< 5%.

Pathway analyses

The pathway data was generated with Ingenuity Pathways Analyses (IPA) software (https://www.qiagenbioinformatics.com/products/ingenuity-pathway-analysis. IPA Summer 2018 Release). The data was mapped into relevant pathways based on their functional annotation and known molecular interactions in Ingenuity's Knowledge Base (IPKB). The -log of p-value were calculated by Fisher's exact test. A data set derived from expression arrays along with the corresponding FC and FDR p-values was uploaded into IPA. The eQTM data set was mapped into relevant pathways in a similar manner.

Immunohistochemistry (IHC)

KI-67 (MIB-1) and PTTG1 (pituitary tumor transformation gene 1) IHCs were performed as described earlier [8]. Other antibodies used were protein tyrosine phosphatase, receptor type D (PTPRD) rabbit Anti-PTPRD (HPA054829, 1:300) (Sigma-Aldrich), protein tyrosine phosphatase, receptor type K (PTPRK) rabbit Anti-PTPRK (HPA054822, 1:400) (Sigma-Aldrich), retinoblastoma (RB1) rabbit Anti-RB1 (HPA050082, 1:500) (Sigma-Aldrich) and anti-Rb (phosphor-S780) (ab47763, 1:70) (Abcam). Anti-mouse/rabbit/rat secondary antibody, Poly-HRP-GAM/R/R (DPVB55HRP, Immunologic) and DAB chromogen (Thermo Fisher Scientific) were used for detection. Ki-67 and PTTG1 scores were obtained by calculating the average percentage of stained cells among the tumor cell population. PTPRD, PTPRD and RB1 proteins were scored by evaluating fractions of immunopositive cells and staining intensities. For scoring details see the Supplementary Methods.

Availability of data and materials

Data has been deposited at the European Genome-phenome Archive (EGA) hosted by the EBI and the CRG, under accession number EGAS00001003488.

RESULTS

Somatic SNV and indel background of *Gsp*- somatotropinomas

The somatic landscape of the tumors ST2-ST12 was reported previously [8]. The tumors had an average of 2.3 coding region SNVs per tumor, with *GNAS* being the only recurrently mutated gene. Here we examined the somatic SNVs and SVs of six additional *Gsp*- tumors: ST13, ST16, ST18-20, and ST22. Supplementary Table S1 gives all the coding region (missense, premature stop codon, frameshift) variants that passed the somatic filtering. These additional *Gsp*- tumors had an excess of somatic variants - in total 92 coding region SNVs and on average 15.3 SNVs per tumor – simply because rare germline variants may have passed the population-

based filtering. The majority of the somatic variants (47 SNVs) arise from ST22 due to patient's Italian ancestry being underrepresented among the population-based controls. Among the 21 tumors studied the only recurrently mutated gene was *GNAS*. No focal deletions or complex chromosomal rearrangements were observed with exception of ST3, a previously reported *Gsp*+ tumor [8] (Supplementary Fig. S1).

SCNA and expression profiling differences in CA- and CS -tumors

Data from 21 somatotropinoma normal/tumor pairs was used for SCNA analysis. Results of eleven normal/tumor pairs were from our earlier work [8]. Analyses revealed that 12 *Gsp*- tumors contained frequent and recurrent (≥4 tumors share the event) chromosomal deletions (chr 1, 4, 6, 14, 15, 16, 18, 22). Also gains (chr 5, 7, 9, 19, 20) of entire chromosomes were detected, although with considerably lower frequency (Supplementary Fig. S1). Copy neutral LOH or homozygous deletions were not observed. All detected chromosomal gains were duplications of a single chromosome. *Gsp*+ tumors contained limited amount of aneuploidy, mostly gains of single chromosomes. An exception was a tumor ST4 with genetic instability (GI%) 22% (Table 1, Supplementary Fig. S1). In addition, two *Gsp*- tumors (ST5 and ST6) were totally aneuploidy-free. GI% did not correlate with clinical variables (Supplementary Table S2). The observed recurrent aneuploidy indicates selective advantage during tumorigenesis rather than random copy number alteration (permutation test $P < 10^{-4}$; Supplementary Fig. S2).

An unsupervised hierarchical clustering analysis of gene expression demonstrated that aneuploidy was the major determinant of somatotropinoma subtypes. Tumors clustered according to the aneuploidy rate as follows (Figure 1A; principal components analysis in Supplementary Fig. S3). Twelve *Gsp*- tumors with aneuploidy, from now on called CA (chromosome aneuploidy)-tumors, clustered together. Accordingly, chromosome stable (CS)-tumors with limited amount or no aneuploidy (7 *Gsp*+ and 2 *Gsp*-) formed their own distinct group. When comparing expressions between CA- and CS-tumors, 881 differentially expressed transcripts (FDR< 5%, |FC|> 2) were identified (Supplementary Table S3). Integration of expression and SCNA data revealed that 69.8% of differentially expressed transcripts locate at chromosomes with recurrent aneuploidy (≥ 4 tumors with shared aneuploidy) from which 81.6% positively correlate with the chromosomal copy number change.

To understand the biological relevance of differentially expressed genes in CA-somatotropinomas, pathway analysis was performed. The top canonical pathway emerged from the tumor subtype-specific expression was

the PKA pathway (Figure 1B, Supplementary Table S4). In this cAMP-mediated signaling pathway a majority of molecules were upregulated in CS-tumor group indicating activated PKA signaling (Figure 2, Table 2). The major inhibitors of cAMP levels [19], phosphodiesterases (PDEs) were up-regulated in CS-tumor group and seven protein tyrosine phosphatase (PTP) receptors were differentially expressed between tumor groups (Table 2).

The expression pathway analysis also highlighted several pathways associated with cell cycle regulation and explicitly in the *retinoblastoma 1*/*E2F transcription factor* (*RB1/E2F*) - mediated G1/S-checkpoint transition. Among the enriched pathways were Molecular Mechanisms of Cancer, Chronic Myeloid Leukemia, Glioma, Glioblastoma Multiforme, and Cell Cycle: G1/S Checkpoint Regulation (Figure 1B, Supplementary Table S4). The genes showing expression differences between tumor groups accumulated in the RB1/E2F -mediated cell cycle regulation and the subsequent G1/S-checkpoint transition indicating difference in mitotic progression (Figure 1C.). *E2F4* transcription factor, a regulator of cell cycle [20], was downregulated in CA-tumor group. By contrast, *histone deacetylase 5* (*HDAC5*) and *RB transcriptional corepressor like 1* (*RBL1*/p107), both repressors of E2F family members, were upregulated in CA-tumor group when compared to CS-tumors. Also the anti-mitogenic growth factor *TGFβ2*/SMAD3 signaling was downregulated in CA-tumor group (Figure 1C, Table 3).

Immunohistochemistry

Because RB1 is the major component of the complex regulating G1/S phase transition, protein levels of total- and phosphorylated-RB1 were semiquantitatively assessed in tumors using immunohistochemistry. In all tumors >90% of nuclei showed positive total- and phospho-RB1 staining. Because fractions of stained cells were comparable between tumor groups, staining intensities were compared. Both tumor groups showed weak to moderate nuclear immunoreactivity of total-RB1 (CA vs CS, 1.67 vs 1.78, $p = 0.6$, Student´s t-test). In addition, some occasional cytoplasmic total-RB1 staining was detected in both tumor groups. Phospho-RB1 showed weak to moderate nuclear staining in both tumor groups (1.59 vs 1.67, $p = 0.71$) (Supplementary Table 5, Supplementary Fig. S4).

To test PKA pathway analysis findings (Figure 2) at the protein levels, PTPRD and PTPRK IHCs were performed. Tumor material was available from four CA- (ST10, ST12, ST18, ST19) and three CS-tumors

(ST15, ST17, ST21). In immunopositive tumors both PTPRD and PTPRK localized mainly in cytoplasm and >90% of cells gave positive staining. PTPRD showed negative immunostaining in CA-tumors (*Gsp*-) and moderate immunoreactivity in CS-adenomas (*Gsp*+). PTPRK immunostaining was negative or weak in CA-tumors and moderate in CS-tumors (Supplementary Fig. 5).

To investigate the role of PTTG1 in the formation of aneuploidy, PTTG1 and Ki-67 immunostainings were performed. Ki-67 and PTTG1 stainings were detected in all tumors. Ki-67 gave nuclear immunostaining. PTTG1 immunopositive cells showed both nuclear and cytoplasmic localization. Most of the cells showed predominant cytoplasmic localization, although there were also cells with predominant nuclear staining in both tumor groups (Supplementary Fig. S6). All stained cells were scored and number of immunopositive cells were significantly more abundant in CA-tumors compared to CS-adenomas ($\bar{x}$ =1.8±1 vs. 0.9±0.5, P=0.016, Wilcoxon-Mann-Whitney) (Table 1). The *PTTG1* RNA expression levels, emerging mainly from non-proliferating cells, were comparable between CA- and CS-tumor groups (FC 1.05, p=0.733). There were no significant difference in Ki-67 scores between tumor groups ($\bar{x}$ =2.7±1.6 vs. 1.7±1.2, P=0.27) (Table 1), but as seen earlier [8, 21] the PTTG1 protein levels correlated with Ki-67 scores (r =0.62, P = 0.002, Pearson`s coefficient).

DNA methylation

We surveyed DNA methylation and differentially methylated regions (DMRs) in 21 somatotropinomas by targeted bisulfite sequencing (Supplementary Table S6). An unsupervised clustering of 50 000 CpG regions with the largest variance between tumors showed, that apart from ST7 and ST21, the tumors clustered according to the *Gsp* mutation status (Figure 3A; principal components analysis in Supplementary Fig. S7). The genome-wide distributions of CpG methylation levels for different genomic contexts revealed that methylation levels of promoter regions were comparable across tumors (Figure 3A). The rest of the annotated regions showed hypomethylation of *Gsp*+ tumors (see below for the supervised analysis of *Gsp*+ and *Gsp*-). Eighteen percentage of the differentially expressed (CA- vs CS) transcripts (119/670 coding transcript clusters; Supplementary Table S3) were correlated with DNA methylation.

DNA methylation patterns are maintained and regulated by DNA methyltransferases (DNMTs), including DNMT1, DNMT3A and DNMT3B [22]. We examined tumor-specific associations of *DNMT* expressions and median CpG methylation and found that CpG methylation rates correlated with the *DNMT1* expression

(Spearman's rank correlation 0.49, p= 0.025) (Supplementary Fig. S8), while *DNMT3A* (0.02, p= 0.929) and *3B* (0.24, p= 0.294) did not show correlation.

DNA methylation associates also with replication timing [17]. Supplementary Fig. S9 shows an overview of CpG methylation at different quartiles of replication timing. Majority of the tumors displayed the expected hypomethylation of late replicating regions (Spearman rho < 0 and P< 0.019; Supplementary Table S7). The *Gsp*- tumors ST10, ST11, ST16, and ST20 had an outstanding, positive correlation to replication time (Spearman rho >0 and P< 0.018), which suggests methylation maintenance also at late replicating regions. No clinical associations were found to explain the methylation maintenance difference in these four tumors (Table 1).

Because the *Gsp* mutation status was the major factor behind the DNA methylation rates and profiles across tumors, DMRs were determined between *Gsp*+ versus *Gsp*- somatotropinomas. Altogether, we found 1 369 DMRs out of which 1 339 (97.8%) were hypomethylated in *Gsp*+ tumors: see Supplementary Table S8 for a complete list of all 1 369 regions' genomic coordinates and annotation of nearby (-20Kbp upstream; 2Kbp downstream) genes (1560 gene annotations). The Supplementary Table S8 is sorted by the absolute value of the test statistic, where negative effect direction denotes hypometylation among the *Gsp*+ tumors compared to the *Gsp*- tumors. Both the outstanding number of DMRs and the enrichment of *Gsp*+ tumors towards hypomethylation can likely be attributed to the genome-wide CpG methylation characteristics between the tumor types (see the unsupervised analysis and Figure 3A). The DMRs did not enrich among the aneuploidy chromosomes; 51% of the DMRs reside at recurrent aneuploidy, while the expected proportion was 55% based on the distribution of the TBS regions.

In addition to the DMR analysis, we also examined the genome-wide methylation profiles between *Gsp*+ and *Gsp*- tumors in different genomic contexts. Supplementary Fig. S10 displays the CpG methylation levels in the context of promoters, enhancers, CpG islands and CCCTC-binding factor (CTCF) sites. The only systematic difference between the *Gsp*+ and *Gsp*- tumors at these genomic contexts was the overall hypomethylation in *Gsp*+ tumors.

To assess the DNA methylation-expression association, the CpG methylation data was integrated with matched transcriptomes by expression quantitative trait methylation (eQTM) analysis [23, 24]. Consistent with previous studies, these associations account for only a small fraction of the assayed CpG sites and expressed genes [24].

In a supervised comparison, the differentially methylated regions between *Gsp*+ and *Gsp*- tumors resulted in a total of 400 DMR regions with significant (FDR< 0.05) expression to methylation eQTMs pertaining 155 genes (Supplementary Table S9; see the Supplementary Fig. S11 for an unsupervised analysis of eQTMs)**.** Altogether, 392 DMR regions (98%), were hypomethylated in *Gsp*+ tumors and from these 333 (84.9%) showed positive eQTM+ association (hypomethylated in *Gsp*+ together with gene underexpression in *Gsp*+). This enrichment can be attributed mostly to the tumor subtype-specific differences in CpG methylation characteristics at gene body regions (Figure 3A).

To identify biological functions associated with the methylation difference between *Gsp*+ and *Gsp*- somatotropinomas, we performed pathway analysis from the eQTM gene list. The majority of emerged pathways (22/31) were associated with inhibitory Gα protein ($G\alpha_i$)– and/or voltage-gated calcium channel (CaCn) signaling (Figure 3B, Supplementary Table S10). Both $G\alpha_i$ and Ca^{2+} signaling are previously connected to pituitary neoplasia [25, 26]. The inhibitory *G protein subunit alpha I-2* (*GNAI2*; $G\alpha_{i\text{-}2}$) and *G protein subunit beta 1* (*GNB1*, $G\beta_1$) were upregulated in *Gsp*+ tumors (Figure 3C, Table 4). The CaCn members, *calcium voltage-gated channel subunit alpha 1A* and *1E* (*CACNA1A* and *CACNA1E*) and *calcium voltage-gated channel auxiliary subunit gamma 2* (*CACNG2*), were downregulated via hypomethylation (Supplementary Table S8).

DISCUSSION

Pituitary tumors are slowly growing benign neoplasia with a low mitotic activity due to senescence. Somatic SNVs and SVs are rarely found in these tumors, indicating that also other mechanisms are driving tumorigenesis [7, 8, 9, 10, 11, 12]. Aneuploidy is a common feature in solid tumors, and it provides cancer cells a mechanism to lose tumor suppressors and gain extra copies of oncogenes [13, 14]. However, a causal relationship between aneuploidy and tumorigenesis as well as genes/pathways that are deregulated by aneuploidy are still incompletely characterized [27]. Aneuploidy is a relatively common event in somatotropinomas [8, 12, 28]. In the current study, we were able to confirm that somatotropinomas create two subtypes associated with distinct aneuploidy rates and unique transcription profiles. The CA-tumor subtype contained *Gsp*- tumors characterized by frequent and recurrent aneuploidy. Recurrent aneuploidy has been associated earlier with more malignant tumors [29], suggesting a selective advantage and role in the tumor

evolution in these cancer types. The other subtype, CS-tumors, contained all *Gsp*+ tumors together with two *Gsp*- adenomas. These tumors were either totally aneuploidy-free or displayed only single chromosome number changes, indicating that expression changes caused by chromosome copy number alterations are poorly tolerated in this tumor subtype.

In some tumor types, aneuploidy is associated with increased malignant potential, tumor recurrence, and drug resistance [13, 14]. In the current study, clinical features of the patients (Supplementary Table S2) did not associate with aneuploidy. Moreover, larger studies have shown that there is no difference in clinical characteristics and outcome of the patients with or without *Gsp* mutation [6, 19], indicating that most aneuploid *Gsp*- tumors do not progress towards aggressive disease.

Because GH-secreting cells constitute only up to 45% of normal anterior pituitary cells [30] and because tumor groups had their own expression signatures (Figure 1A), expression profile comparison was performed between CA- and CS-tumor groups. Moreover, there was not normal anterior pituitary lobe tissue available for the study. Differentially expressed genes in CA- and CS-tumors enriched most significantly in the PKA signaling. It is well established that oncogenic *Gsp* mutations activate the cAMP-dependent PKA pathway [5]. Therefore this result reflects the *Gsp*+ tumor-induced activation of PKA signaling in the CS-tumor group. In addition to the previously *Gsp*+ tumor - associated molecules, e.g. cAMP-specific PDEs [19], we found that many protein tyrosine phosphatase (PTPs) receptors were differentially expressed in CA- and CS-tumor groups. Moreover, PTPRD and PTPRK IHCs showed elevated protein levels in *Gsp*+ tumors. PTPs are known to regulate crosstalk between cAMP and the mitogen-activated protein (MAP) kinase cascade [31], and abundant enrichment of these genes imply the role for the PTP-signaling in the tumorigenesis of *Gsp*+ adenomas.

RB1/E2F complex has a major role in the cell cycle regulation. It controls the G1/S phase transition during the cell cycle and is regulated by the RB1 pocket proteins (RB1, RBL1/p107, RBL2/p130) and E2F transcription factors. Dysregulated G1/S-phase transition promotes tumor formation and may give rise to aneuploidy. Inactivation of RB1 through phosphorylation leads release of E2F transcription factors and subsequent cell cycle progression. RB1/E2F complex has shown to be involved in pituitary tumorigenesis. *RB1* is a tumor suppressor and mice with heterozygous inactivating *Rb1* mutation develop pituitary adenomas [20, 32, 33]. Our expression data showed that RB1/E2F-mediated G1/S –checkpoint signaling is differentially regulated

between the tumor groups. The CA-tumor group displayed downregulation of *E2F4*, whereas *E2F*-repressors *HDAC5* and *RBL1*/p107 [34] were upregulated. *E2F4* is traditionally categorized as a transcriptional repressor, but more recently it was shown that in some tissue types *E2F4* may act as an activator of proliferation [35]. The function of *E2F4* in GH-secreting pituitary cells is not elucidated. Interestingly, apart from *HDAC5* (17q21), all differentially expressed G1/S- related genes, *E2F4* (16q22), *RBL1* (20q11), and *TGF-β2 (*1q41), *SMAD3* (15q.22) locate on chromosomes with recurrent aneuploidy and their expression correlated with the direction of aneuploidy (Supplementary Fig. S1).We did not observed differences in protein levels of tot- and phospho-RB1 between CA- and CS-tumor groups. Immunohistochemistry is, however, a semiquantitative method and do not necessary detect more subtle protein level differences.

The pituitary tumor-transforming 1 gene (*PTTG1*) (5q33) is a mitotic checkpoint protein which regulates a sister chromatid segregation during mitosis as well as genes encoding G1/S and G2/M phase proteins [36, 37, 38]. RNA and protein levels of PTTG1 exhibit a cell cycle–dependent expression pattern, being highest at G2/M phase and attenuated after mitosis. *PTTG1* is expressed in all types of pituitary tumors [39, 40]. Mice with overexpressed *Pttg1* develop pituitary adenomas, whereas knockout $Pttg1^{-/-}$ animals do not [41, 42]. Crossbreeding of overexpressed *Pttg1* animal with heterozygous $Rb1^{+/-}$ mice increased penetrance of pituitary tumors. In contrast, crossbreeding of $Pttg1^{-/-}$ animals with $Rb1^{+/-}$ mice showed decreased tumor number and size, further supporting cooperative relationship between PTTG1 and RB1 in pituitary tumorigenesis [41, 42, 43]. It has also shown that both loss and overexpression of *PTTG1* promote aneuploidy and G1/S cell cycle arrest induced senescence [43, 44, 45].

We showed that CA-tumors with recurrent aneuploidy exhibit higher PTTG1 protein levels. This finding together with the known function of PTTG1 in pituitary tumorigenesis [36, 39, 41, 43**,** 44] may indicate that elevated PTTG1 levels are involved in the development of aneuploidy in CA-somatotropinomas. During the initial steps of tumorigenesis, slowly accumulating aneuploidy can mediate excessive proliferation by changing gene expressions and modulating functions of pituitary tumor driver pathways. Eventually, however, recurrent aneuploidy leads to mitotic stress and senescence via altered levels of proteins involved in the RB1/E2F– mediated G1/S cell cycle progression. Thus, in CA-somatotropinomas aneuploidy may underlie both the tumor formation as well as escape from aggressive growth and malignancy.

Interestingly, *PTTG1* seems to be a downstream target of E2F transcription factor family [33]. However, the regulatory mechanisms of *PTTG1* are only partially elucidated and further studies are required in order to evaluate the role of PTTG1 in pituitary tumorigenesis.

Alterations of DNA methylation have been recognized as an important component of tumor development and progression of cancer through different mechanisms. It has been shown, that pituitary tumors have their own distinct DNA methylation profile without overlapping with other sellar region tumors [12]. The current work shows that DNA methylation of somatotropinomas tends to cluster according to the *Gsp* mutation status. DNA methylation levels can have longitudinal changes due to epigenetic reprogramming during tumorigenesis [46], which may explain the observed mis-clusterd tumors in our sample set. In general, *Gsp*+ tumors were hypomethylated when compared to *Gsp*- tumors and distributions of methylation levels for different genomic contexts across tumors revealed distinct *Gsp* genotype-specific methylation profiles. DNMT1 is a methyltransferase enzyme, which maintains DNA methylation during cell replication. Aberrant expression of *DNMT1* is involved in tumor transformation and progression in many cancer types [22, 47]. In the present study, expression of *DNMT1* was found to be positively correlated with tumor-specific methylation levels, indicating involvement of *DNMT1* in the somatotropinoma tumorigenesis through establishment of methylation levels.

Gsp genotype-specific DNA methylation profiles indicate that different molecular mechanisms are involved in the development and progression of *Gsp*+ and *Gsp*- pituitary tumors. The integration of DNA methylation and gene expressions demonstrated that the inhibitory Gα protein ($G\alpha_i$) signaling, together with the voltage-gated calcium channel (CaCn) transducer signaling are the major biological functions differentially regulated via DNA methylation in these tumor subtypes. In *Gsp*+ tumors $G\alpha_i$ signaling was activated through overexpression of $G\alpha_{i\text{-}2}$ (*GNAI2*) and Gβ1 (*GNB1*), whereas CaCn subunits were downregulated. Both of these signaling cascades are involved in the regulation of cAMP response. Inhibitory $G\alpha_i$ proteins most notably inhibit receptor-dependent cAMP synthesis [48]. CaCn signaling stimulates the cAMP response element-binding (CREB) protein, a main downstream target of mitogenic effect of cAMP [26, 49, 50]. Thus, activated $G\alpha_i$ and downregulated CaCn emphasize the adaptive response to elevated cAMP levels caused by *GNAS* ($G\alpha_s$) mutation and hereby likely prevents the excessive cellular proliferation in *Gsp*+ tumors. We have earlier shown that dysfunctional $G\alpha_i$ signaling and particularly the reduced $G\alpha_{i\text{-}2}$ protein levels contribute to the development

of *AIP* germline mutation associated somatotropinomas [25]. This study, however, shows for the first time the essential role of $G\alpha_i$ signaling in *Gsp*+ somatotropinomas with constitutively activated cAMP synthesis.

The systematic characterization of the somatic landscape using genomic, epigenomic, and transcriptomic data across *Gsp*+ and *Gsp*- somatotropinomas highlighted tumor subtypes and subtype-specific mechanisms of tumorigenesis. The study suggest association between increased PTTG1 protein levels and aneuploidy in *Gsp*- adenomas, whereas *Gsp*+ tumors are characterized by DNA methylation controlled $G\alpha_i$ – CaCn signaling, a response to the mitogenic cAMP-signaling caused by *GNAS* mutation. While further studies are needed to fully characterize the molecular mechanisms resulting from aneuploidy-induced pituitary tumorigenesis, the work presented here provides valuable new information about subtype-specific pituitary tumorigenesis. Moreover, these findings may help to elucidate the mechanisms of aneuploidy also in other tumor types.

Authors' Contributions

Conception and design: N. Välimäki, A. Karhu

Development of methodology: N. Välimäki

Acquisition of data (provided animals, acquired and managed patients, provided facilities, etc.): C. Schalin-Jäntti, A. Karppinen, L. Kivipelto, L.A. Aaltonen

Analysis and interpretation of data (e.g., statistical analysis, biostatistics, computational analysis): N. Välimäki, A. Paetau, A. Karhu

Writing, review, and/or revision of the manuscript: N. Välimäki, C. Schalin-Jäntti, A. Karppinen, L. Kivipelto, L.A. Aaltonen, A. Karhu

Administrative, technical, or material support (i.e., reporting or organizing data, constructing databases): N. Välimäki, C. Schalin–Jäntti, L.A. Aaltonen, A. Karhu

Study supervision: A. Karhu

Acknowledgements

We thank Heikki Metsola, Sini Marttinen, Alison Ollikainen, Marjo Rajalaakso, Inga-Lill Åberg and Iina Vuoristo for technical assistance. We acknowledge the computational resources provided by the ELIXIR node hosted at CSC - IT Center for Science, Finland. The Biomedicum Imaging Unit (BIU) for the microscopy service and Biomedicum Functional Genomics Unit (FuGU) for the microarray services are acknowledged.

References

1. Daly AF, Rixhon M, Adam C, Dempegioti A, Tichomirowa MA, Beckers A. High prevalence of pituitary adenomas: a cross-sectional study in the province of Liege, Belgium. J Clin Endocrinol Metab 2006;91:4769-75.
2. Dekkers OM, Biermasz NR, Pereira AM, Romijn JA, Vandenbroucke JP. Mortality in acromegaly: a metaanalysis. J Clin Endocr Metab 2008;93:9361–67.
3. Melmed S. Acromegaly pathogenesis and treatment. J Clin Invest 2009;119:3189–202.
4. Ritvonen E, Löyttyniemi E, Jaatinen P, Ebeling T, Moilanen L, Nuutila P, *et al.* Mortality in acromegaly: a 20-year follow-up study. Endocr Relat Cancer 2016;23:469-80.
5. Vallar L, Spada A, Giannattasio G. Altered Gs and adenylate cyclase activity in human GH-secreting pituitary adenomas. Nature 1987;330:566-8.
6. Ritvonen E, Pitkanen E, Karppinen A, Vehkavaara S, Demir H, Paetau A, *et al.* Impact of AIP and inhibitory G protein alpha 2 proteins on clinical features of sporadic GH-secreting pituitary adenomas. Eur J Endoc 2017;176: 243-52.
7. Newey PJ, Nesbit MA, Rimmer AJ, Head RA, Gorvin CM, Attar M, *et al.* Whole-exome sequencing studies of nonfunctioning pituitary adenomas. J Clin Endocrinol Metab 2013;98:E796-E800.
8. Välimäki N, Demir H, Pitkänen E, Kaasinen E, Karppinen A, Kivipelto L, *et al.* Whole-Genome Sequencing of Growth Hormone (GH)-Secreting Pituitary Adenomas. J Clin Endocrinol Metab 2015;100:3918-27.
9. Lan X, Gao H, Wang F, Feng J, Bai J, Zhao P, *et al*. Whole-exome sequencing identifies variants in invasive pituitary adenomas. Oncology Lett 2016;12:2319-28.
10. Song ZJ, Reitman ZJ, Ma ZY, Chen JH, Zhang QL, Shou XF, *et al.* The genome-wide mutational landscape of pituitary adenomas. Cell Res 2016;26:1255-9.
11. Ronchi CL, Peverelli E, Herterich S, Weigand I, Mantovani G, Schwarzmayr T, *et al.* Landscape of somatic mutations in sporadic GH-secreting pituitary adenomas..Eur J Endocrinol 2016;174:363-72.
12. Capper D, Jones DTW, Still M, Hovestadt V, Schrimpf D. Sturm D. et al. DNA methylation-based classification of central nervous system tumours. Nature 2018;555:469-74.

13. Carter SL, Eklund AC, Kohane IS, Harris LN, Szallasi Z. A signature of chromosomal instability inferred from gene expression profiles predicts clinical outcome in multiple human cancers. Nat Genet 2006;38:1043–8.
14. Weaver BA, Cleveland DW. Does aneuploidy cause cancer? Curr Opin Cell Biol 2006;18:658-67.
15. Farrell WE. Epigenetics of pituitary tumours: an update. Curr Opin Endocrinol Diabetes Obes 2014;21:299–305.
16. Karolchik D, Hinrichs AS, Furey TS, Roskin KM, Sugnet CW, Haussler D. *et al.* The UCSC Table Browser data retrieval tool. Nucleic Acids Res 2004;32:D493–96.
17. Chen CL, Rappailles A, Duquenne L, Huvet M, Guilbaud G, Farinelli L. *et al.* Impact of replication timing on non-CpG and CpG substitution rates in mammalian genomes. Genome Res 2010;20:447-57.
18. Shabalin AA. Matrix eQTL: Ultra fast eQTL analysis via large matrix operations. Bioinformatics 2012;28:1353-58.
19. Peverelli E, Mantovani G, Lania AG, Spada A. cAMP in the pituitary: an old messenger for multiple signals. J Mol Endocrinol 2013;52:R67–R77.
20. Manning AL, Dyson NJ. RB: mitotic implications of a tumour suppressor. Nat Rev Cancer 2012;12:220– 6.
21. Filippella M, Galland F, Kujas M, Young J, Faggiano A, Lombardi G, *et al.* Pituitary tumour transforming gene (PTTG) expression correlates with the proliferative activity and recurrence status of pituitary adenomas: a clinical and immunohistochemical study. Clin Endocrinol 2006;65:563-43.
22. Robertson KD, Keyomarsi K, Gonzales FA, Velicescu M, Jones PA. "Differential mRNA expression of the human DNA methyltransferases (DNMTs) 1, 3a and 3b during the G(0)/G(1) to S phase transition in normal and tumor cells". Nuc Acids Res 2000; 28:2108–13.
23. Kulis M, Heath S, Bibikova M, Queiros AC, Navarro A, Clot G *et al*. Epigenomic analysis detects wide-spread gene-body DNA hypomethylation in chronic lymphocytic leukemia. Nat Genet 2012;44:1236-42.

24. Gutierrez-Arcelus M, Lappalainen T, Montgomery SB, Buil A, Ongen H, Yurovsky A, *et al.* Passive and active DNA methylation and the interplay with genetic variation in gene regulation. eLife 2013;2:e00523.
25. Tuominen I, Heliövaara E, Raitila A, Rautiainen M, Mehine M, Katainen R, *et al*. AIP inactivation leads to pituitary tumorigenesis through defective Gαi-cAMP signaling. Oncogene 2015;34:1174-84.
26. Nussinovitch I. Ca^{2+} channels in anterior pituitary somatotrophs: A therapeutic perspective. Endocrinol 2018;159:4043–55.
27. Beroukhin R, Mermel CH, Porter D, Wei G, Raychaudhuri S, Donovan J, *et al.* The landscape of somatic copy-number alteration across human cancers. Nature 2010;463:899-905.
28. Salomon MP, Wang X, Marzese DM, Hsu SC, Nelson N, Zhang X, *et al.* The Epigenomic Landscape of Pituitary Adenomas Reveals Specific Alterations and Differentiates Among Acromegaly, Cushing's Disease and Endocrine-Inactive Subtypes. Clin Cancer Res 2018;24:4126-36.
29. Knouse KA, Davoli T, Elledge SJ, Amon A. Aneuploidy in cancer: Seq-ing answers to old questions. Annu Rev Cancer Biol 2017;1: 335-54.
30. Bonert VS, Melmed S. Growth Hormone. The Pituitary (Fourth Edition) 2017; 85-127.
31. Saxena M, Williams S, Taskén K. Mustelin T. Crosstalk between cAMP-dependent kinase and MAP kinase through a protein tyrosine phosphatase. Nature Cell Biol 1999;1:305–10.
32. Jacks T, Fazeli A, Schmitt EM, Bronson RT, Goodell MA, Weinberg RA. Effects of an Rb mutation in the mouse. Nature 1992; 359: 295–300.
33. Zhou C, Wawrowsky K, Bannykh S, Gutman S, Melmed S. E2F1 induces pituitary tumor transforming gene (PTTG1) expression in human pituitary tumors. Mol Endocrinol 2009;23:2000–12
34. Dyson, N. The regulation of E2F by pRB-family proteins. Genes Develop 1998;12:2245-62.
35. Crosby ME, Almasan A. Opposing roles of E2Fs in cell proliferation and death. Cancer Biol Ther 2004;3:1208-11.
36. Romero F, Multon M-C, Ramos-Morales F, Domínguez Á, Bernal JA, Pintor-Toro JA, *et al.* Human securin, hPTTG, is associated with Ku heterodimer, the regulatory subunit of the DNA-dependent protein kinase. Nucleic Acids Res 2001;29:1300–07.

510 37. Pascreau G, Arlot-Bonnemains Y, Prigent C. Phosphorylation of histone and histone-like proteins by
511 aurora kinases during mitosis. Prog Cell Cycle Res 2003;5:369–74.
512 38. Tong Y, Tan Y, Zhou C, Melmed S. Pituitary tumor transforming gene interacts with Sp1 to modulate
513 G1/S cell phase transition. Oncogene 2007;26:5596–605.
514 39. Uccella S, Tibiletti MG, Bernasconi B, Finzi G, Oldrini R, Capella C. Aneuploidy, centrosome
515 alteration and securin overexpression as features of pituitary somatotroph and lactotroph adenomas.
516 Anal Quant Cytol Histol 2005;27:241-52.
517 40. Vlotides G, Eigler T, Melmed S. Pituitary Tumor-Transforming Gene: Physiology and Implications
518 for Tumorigenesis. Endo Rev 2007;28:165–186.
519 41. Abbud RA, Takumi I, Barker EM, Ren SG, Chen DY, Wawrowsky K *et al.* Early multipotential
520 pituitary focal hyperplasia in the alpha-subunit of glycoprotein hormone-driven pituitary tumor-
521 transforming gene transgenic mice. Mol Endocrinol 2005;19: 1383 –91.
522 42. Donangelo I, Gutman S, Horvath E, Kovacs K, Wawrowsky K, Mount M, *et al*. Pituitary tumor
523 transforming gene overexpression facilitates pituitary tumor development. Endocrinology
524 2006;147:4781–91.
525 43. Chesnokova V, Zonis S, Rubinek T, Yu R, Ben-Shlomo A, Kovacs K, *et al.* Senescence mediates
526 pituitary hypoplasia and restrains pituitary tumor growth. Cancer Res 2007;67:10564-72**.**
527 44. Yu R, Lu W, Chen J, McCabe CJ, Melmed, S. Overexpressed pituitary tumor-transforming gene
528 causes aneuploidy in live human cells. Endocrinology 2003;144:4991–8.
529 45. Kim D, Pemberton H, Stratford AL, Buelaert K, Watkinson JC, Lopes V, *et al.* Pituitary tumour
530 transforming gene (PTTG) induces genetic instability in thyroid cells. Oncogene 2005;24:4861–6.
531 46. Doi A, Park IH, Wen B, Murakami P, Aryee MJ, Irizarry R, *et al.* Differential methylation of tissue-
532 and cancer-specific CpG island shores distinguishes human induced pluripotent stem cells, embryonic
533 stem cells and fibroblasts". Nat Genet 2009;41:1350–53.
534 47. Feinberg AP, Koldobskiy MA, Gondor A. Epigenetic modulators, modifiers and mediators in cancer
535 aetiology and progression. Nat Rev Genet 2016;17:284–99.

536 48. Nürnberg B, Gudermann T, Schultz G. Receptors and G proteins as primary components of
537 transmembrane signal transduction. Part 2. G proteins: structure and function. J Mol Med
538 1995;73:123–32.
539 49. Bertherat J, Chanson P, Montminy M. The cyclic adenosine 3`,5`-monophospate-responsive factor
540 CREB is constitutively activated in human somatotroph adenomas. Mol Endocrinol 1995;9:777-83.
541 50. Shaywitz, AJ, Greenberg ME. “CREB: A Stimulus-Induced Transcription Factor Activated by A
542 Diverse Array of Extracellular Signals". Ann Rev Biochem 1999;68:821–61

Authors´contributions

NV processed, analyzed, and consolidated the data, provided statistical analyses, and contributed to the writing of the manuscript. **CS-J** supported in the blood and tumor sample collections, provided the clinical and laboratory parameters as well as the different treatments given to the patients, interpreted the clinical data, and contributed to the writing of the manuscript. **LK** and **AtK** contributed to the blood and the tumor sample collections for the study, and work with the manuscript preparation. **AP** provided pathological reviews for the study. **LAA** provided support for the data collection, aided in interpreting the results, and worked on the manuscript. **AK** analyzed and interpreted the data, provided statistical analysis, and contributed to the writing of the manuscript. All authors read and approved the manuscript.

SUPPLEMENTARY DATA:

Supplementary Methods – Supplementary text containing details about mutation status validation of established pituitary adenoma predisposing genes and IHC scoring.

Supplementary Tables - Supplementary Tables S1-S10 shows: 1) All the coding region variants (missense, premature stop codon, frameshift) of 21 sequenced somatotropinomas that passed the somatic filtering. 2) Results of correlation tests between genetic instability (GI%) and clinical variables. 3) Differentially expressed transcripts (FDR ≤ 5%, FC -2 ≥ x ≥ 2) in CA- and CS-tumors. 4) Significantly enriched canonical pathways carried out from differentially expressed genes (FDR < 5% and |FC|> 2; CA- vs CS-tumors). 5) Immunostaining intensities of total- and phosphorylated-RB1 in CA- and CS-tumors. 6) CpG quality statistics. 7) Replication timing and CpG methylation. 8) Differentially methylated regions (DMRs) between *Gsp*+ versus *Gsp*- tumors, and nearby genes. 9) Integration of DMRs with matched transcriptomes by expression quantitative trait methylation (eQTM) analysis (at 5% FDR). 10) The complete list of significantly ($p< 0.05$) enriched cis-eQTM pathways.

Supplementary Figures - Supplementary Figures S1-9 show 1) Overview of the somatic copy-number aberrations. 2) Enrichment of whole-chromosome deletions and amplifications. 3) Principal component analysis of expression array data. 4) Total (tot) and phsoporylated (p) RB1 inmmunohostochemistry in CA- and CS-tumors. 5) PTPR and PTPRK immunohistochemistry in CA- and CS-tumors. 6) Ki-67- and PTTG1

570 immunostainings. 7) Principal component analysis of CpG methylation estimates. 8) *DNMT1* and genome-
571 wide methylation. 9) Replication timing and CpG methylation. 10) Context-specific characteristics of CpG
572 methylation estimates. 11) Unsupervised analysis of expression quantitative trait methylation (eQTM).

573

Table 1. Characteristics of the patients. IGF-1 and PRL levels at diagnosis were compared to age- and sex-matched upper normal limits

Patient	Age at diagnosis /Gender	Elevated pituitary hormone	IGF-1 (% of UNL)	PRL (% of UNL)	Tumor size	*Gsp* status	No of surgeries	Radiotherapy	Current medical therapy	GI (%)	Ki-67 (%±SD)	PTTG1 (%±SD)
ST2[a]	43/M	GH	329		macro	R201C	1	no	NA	4.9	0.9±0.17	0.5±0.21
ST3[a]	37/M	GH/PRL	458	1340	macro	R201C	2	yes	yes	0	3.8±0.44	0.6±0.19
ST4[a]	69/F	GH	207		micro	R201C	1	no	no	22	1.7±0.4	0.5±0.39
ST5[a]	56/M	GH	177		macro	-	1	no	no	0	2.4±0.7	1.1±0.32
ST6[a]	40/M	GH	313		macro	-	1	yes	yes	0	1.9±0.35	0.9±0.12
ST7[a]	40/F	GH	189		macro	-	2	yes	NA[b]	34.1	3.5±0.31	1.7±0.38
ST8[a]	55/F	GH	187		macro	-	1	no	NA	34.1	1.2±0.44	0.9±0.40
ST9[a]	38/F	GH	202		macro	-	1	no	no	41.5	3.4±0.77	0.9±0.24
ST10[a]	14/M	GH	14		macro	-	1	no	no	41.5	6.4±0.71	3.1±0.44
ST11[a]	24/F	GH	138		macro	-	2	yes	no	43.9	1.8±0.54	1±0.34
ST12[a]	37/M	GH	305		macro	-	2	no	yes	58.5	0.5±0.46	0.3±0.13
ST13	40/M	GH	247		macro	-	1	no	yes	32.1	1.4±0.47	1.7±0.43
ST14	59/M	GH	NA		NA	R201C	1	no	NA	0	0.5±0.45	0.7±0.26
ST15	62/F	GH	374		macro	R201C	1	no	NA	5.1	1.4±0.48	0.6±0.31
ST16	59/M	GH	57		macro	-	1	no	yes	43.6	1.0±0.42	1.7±0.27
ST17	45/M	GH	38		macro	Q227L	1	no	yes	0	0.6±0.19	0.8±0.22
ST18	26/F	GH	78		macro	-	1	no	no	46.2	4.1±0.64	2.6±0.30
ST19	53/F	GH	177		macro	-	1	no	yes	10.3	2.7±0.35	3.7±0.40
ST20	44/M	GH	135		micro	-	1	no	no	46.2	3.1±0.30	2.6±0.52
ST21	34/M	GH	274		macro	Q227L	1	no	yes	2.6	2.8±0.44	2.1±0.49
ST22	37/M	GH	234		macro	-	1	no	no[b]	25.6	1.9±0.37	1.5±0.39

574 Abbreviation: M, male; F, female; GH, growth hormone; PRL, prolactin; IGF-1, insulin-like growth factor 1;
575 % of UNL, percent increase compared to upper normal limit; G*sp* status, mutation observed; GI, genetic
576 instability; PTTG1, pituitary tumor transforming gene 1. [a]WGS and SCNA data of tumors published in
577 Välimäki *et al*. [8]. NA, not available; [b]non-compliant, not in remission

Table 2. Differentially expressed genes in the PKA Signaling pathway (CA- vs CS-tumors).

Symbol	Entrez Gene Name	FC	FDR	Type	Symbol in Pathway
AKAP13	A-kinase anchoring protein 13	-2.820	0.017	other	AKAP
CAMK2D	calcium/calmodulin dependent protein kinase II delta	2.210	0.038	kinase	CAMK2
EYA1	EYA transcriptional coactivator and phosphatase 1	-6.640	0.021	phosphatase	PTP
NFAT5	nuclear factor of activated T-cells 5	-2.060	0.005	transcription regulator	NFAT
PDE10A	phosphodiesterase 10A	-2.840	0.042	enzyme	PDE
PDE4D	phosphodiesterase 4D	-2.660	0.026	enzyme	PDE
PDE7B	phosphodiesterase 7B	-4.840	0.001	enzyme	PDE
PHKB	phosphorylase kinase regulatory subunit beta	-3.370	0.000	kinase	PHK
PLCL1	phospholipase C like 1 (inactive)	-4.660	0.002	enzyme	PLC
PRKCD	protein kinase C delta	3.310	0.035	kinase	PKC
PTPRD	protein tyrosine phosphatase, receptor type D	-22.200	0.003	phosphatase	PTP
PTPRE	protein tyrosine phosphatase, receptor type E	-2.690	0.033	phosphatase	PTP
PTPRG	protein tyrosine phosphatase, receptor type G	-6.560	0.002	phosphatase	PTP
PTPRH	protein tyrosine phosphatase, receptor type H	3.220	0.011	phosphatase	PTP
PTPRJ	protein tyrosine phosphatase, receptor type J	3.810	0.026	phosphatase	PTP
PTPRK	protein tyrosine phosphatase, receptor type K	-7.020	0.007	phosphatase	PTP
PTPRS	protein tyrosine phosphatase, receptor type S	3.100	0.047	phosphatase	PTP
RAP1A	RAP1A, member of RAS oncogene family	-2.000	0.013	enzyme	RAP1
RYR2	ryanodine receptor 2	-7.880	0.001	ion channel	RYR
SMAD3	SMAD family member 3	-8.770	0.011	transcription regulator	SMAD3
TCF4	transcription factor 4	-2.450	0.013	transcription regulator	TCF/LEF
TGFB2	transforming growth factor beta 2	-2.120	0.046	growth factor	TGF-β

FC: expression fold change; FDR: false discovery rate

578

579

Table 3. G1/S Checkpoint Regulation enriched genes from expression pathway analysis (CA- vs. CS-tumors).

Symbol	Entrez Gene	FC	FDR	Type	Symbol in Pathway
E2F4	E2F transcription factor 4	-2.230	0.030	transcription regulator	E2F
HDAC5	histone deacetylase 5	2.180	0.004	transcription regulator	HDAC
RBL1	RB transcriptional corepressor like 1	2.080	0.006	transcription regulator	RBL1 (p107)
RBBP8	RB binding protein 8, endonuclease	-4.06	0.004	enzyme	RBBP8
SMAD3	SMAD family member 3	-8.770	0.010	transcription regulator	SMAD3
TGF-β2	transforming growth factor-β2	-2.120	0.045	growth factor	TGF-β

FC: expression fold change; FDR: false discovery rate

580

Table 4. Differentially regulated genes in the CREB Signaling pathway (*Gsp*+ vs. *Gsp*-).

Symbol	Entrez Gene	eQTMβ	FDR	Type	Symbol in Pathway
CACNA1A	calcium voltage-gated channel subunit alpha1 A	3.77	0.001	ion channel	CaCn
CACNA1E	calcium voltage-gated channel subunit alpha1 E	1.73	0.019	ion channel	CaCn
CACNG2	calcium voltage-gated channel auxiliary subunit gamma 2	5.25	0.001	ion channel	CaCn
GNAI2	G protein subunit alpha i2	-1.17	0.016	ion channel	Gα/Gαi
GNB1	G protein subunit beta 1	-1.40	0.021	ion channel	Gβ

eQTMβ: Expression quantitative trait methylation, a correlation between gene expression and methylation, FDR: false discovery rate

581

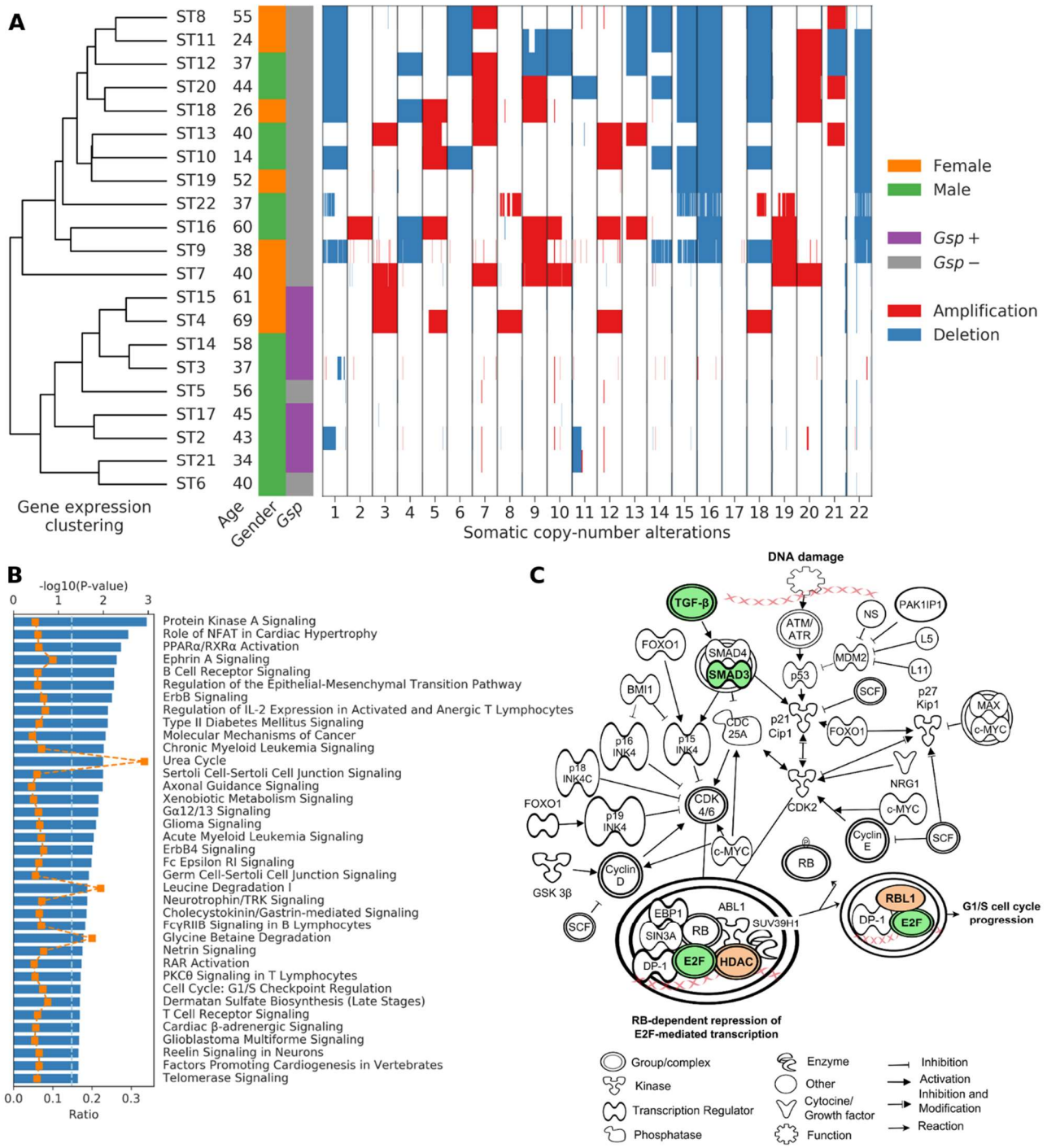

582

583 **Figure 1**. **A**, Gene expression of somatotropinomas clustered according to the aneuploidy rate. Left: Result of
584 unsupervised hierarchical clustering of expression-array data from 21 somatotropinomas. Middle: Patients'
585 age at diagnosis, gender, and *Gsp* mutation status. Right: Somatic copy-number aberrations**.** Supplementary:
586 Fig. S1 shows all somatic chromosomal aberrations in more detail. Of note, the chr 1p of ST3 contains
587 chromothripsis event [8]. **B**, Enriched pathways result from differentially expressed genes (CA- vs CS-tumors).
588 Supplementary Table S4 shows the complete list of significantly ($p < 0.05$) enriched expression pathways and

genes. The blue horizontal bars denote the association P-values for each pathway on a logarithmic scale (dashed vertical line at p=0.05). The ratio between the number of query genes found and total number of genes in a pathway is shown in orange. **C**, The enriched G1/S Signaling pathway. The colored molecules identified as differentially regulated in CA- vs CS-tumor groups. FCs and p-values are listed in Table 3. Orange label=up-regulated; green label = down-regulated.

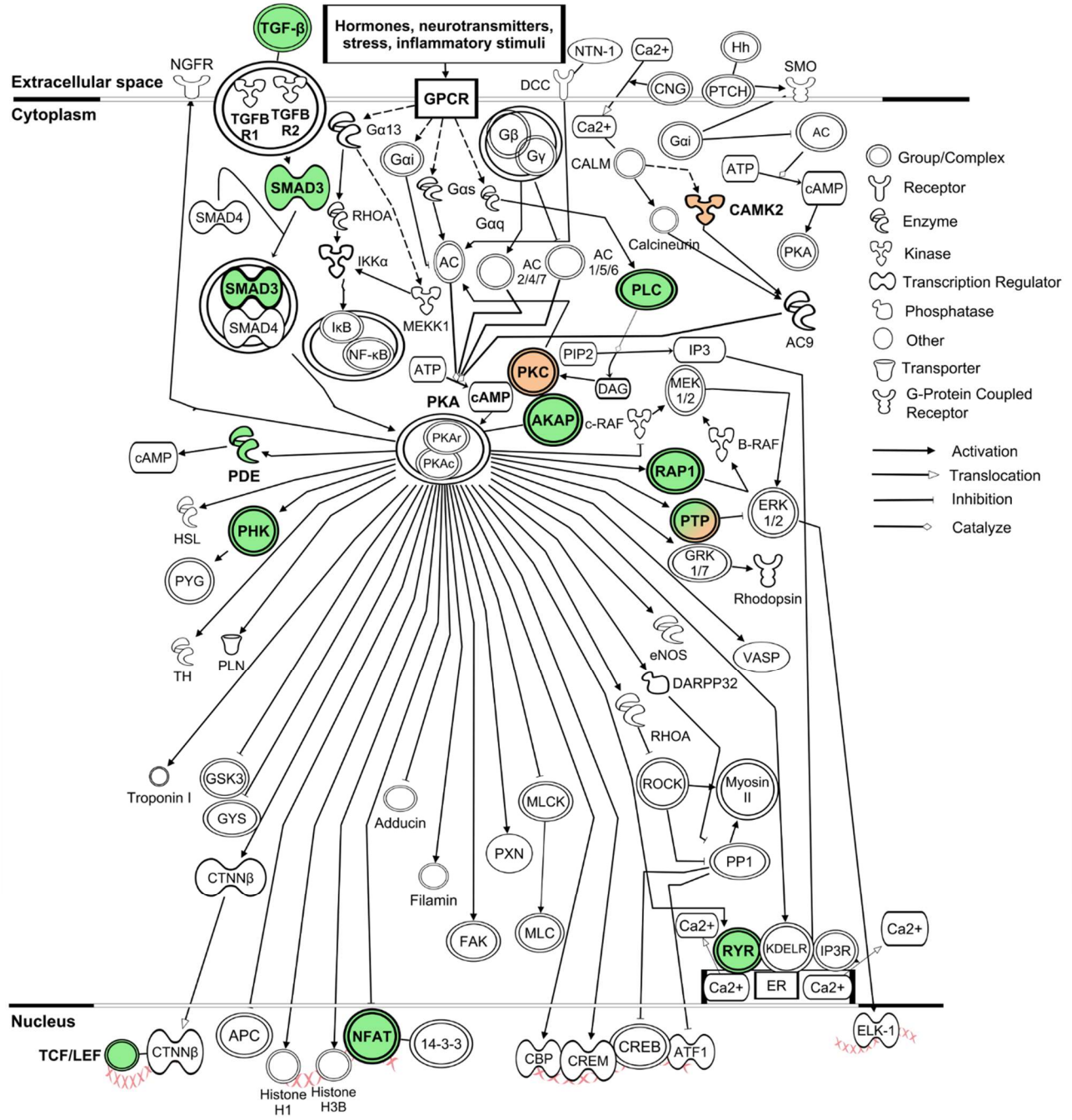

Figure 2. The enriched PKA Signaling pathway. The colored molecules identified as differentially expressed genes or gene groups in CA- vs CS-tumors. FCs and p-values are listed in Table 2. Orange label=up-regulated; green label = down-regulated.

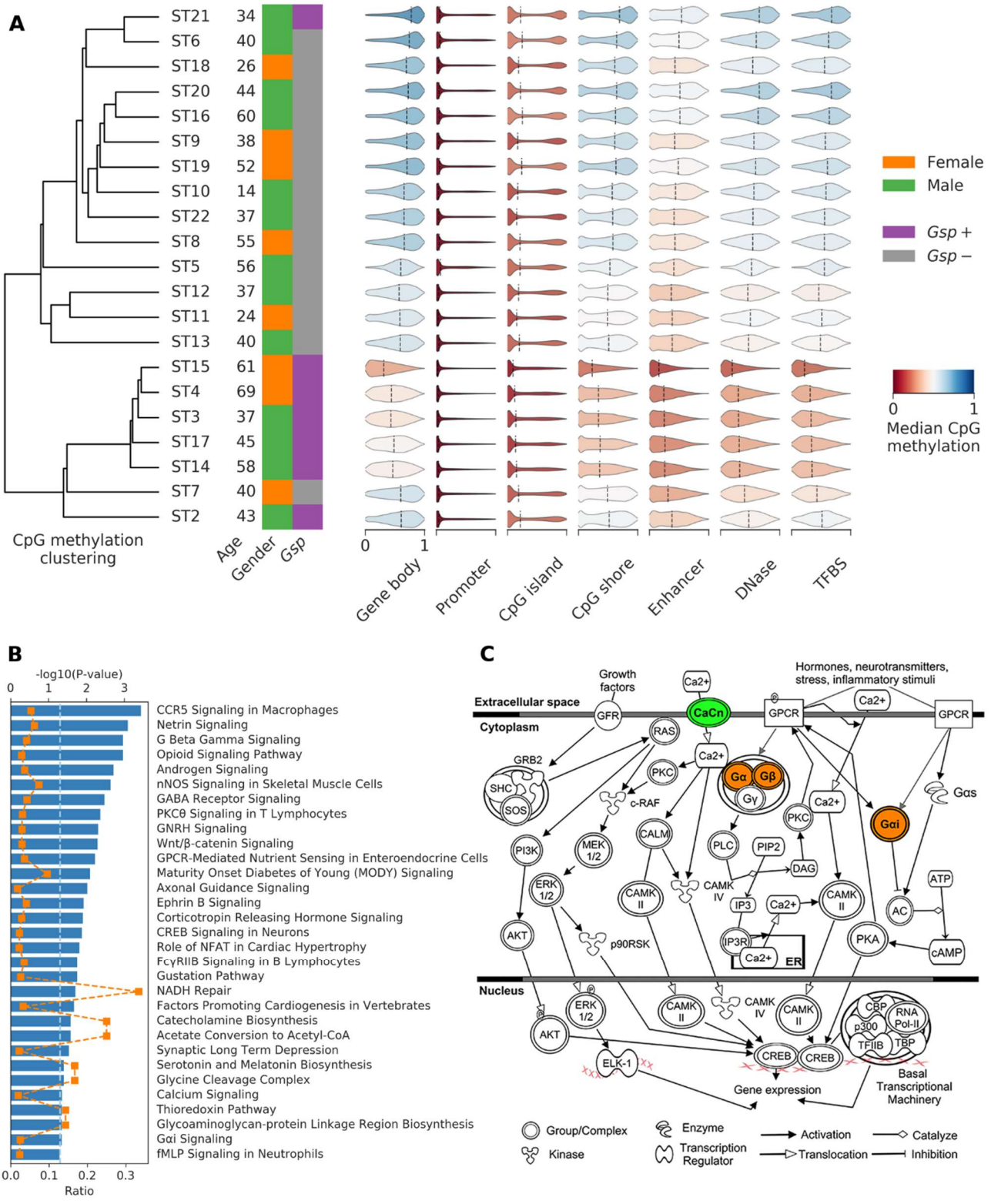

Figure 3. **A**, CpG methylation of somatotropinomas clustered according to the *Gsp* mutation status. Left: Unsupervised hierarchical clustering of CpG methylation data from 21 somatotropinoma samples (based on 50 000 regions with the largest variance between tumors). Middle: Patient's age at diagnosis, gender, and *Gsp* mutation status. Right: Distribution of estimated CpG methylation levels for each genomic context: gene body

603 (from +2kb relative to the TSS to the end of gene), promoter (-1kb to +2kb relative to the TSS), CpG
604 island/shore, enhancer, DNase (DNaseI Hypersensitivity Cluster), and TFBS (Transcription factor cluster) (see
605 Materials and methods for details). Methylation levels are quantified by value ranging from zero
606 (unmethylated) to one (fully methylated)**. B**, Pathway analyses from cis-eQTMs. Supplementary Table S10
607 shows the list of significantly ($p < 0.05$) enriched cis-eQTM pathways and genes. The blue horizontal bars
608 denote the association P-values for each pathway on a logarithmic scale (dashed vertical line at $p=0.05$). The
609 ratio between the number of query genes found and total number of genes in a pathway is shown in orange. **C**,
610 The enriched CREB Signaling in Neurons pathway. The colored molecules identified as differentially
611 expressed *Gsp*+ vs *Gsp*- tumors. eQTM- and FDR-values are listed in Table 4. Orange label=up-regulated;
612 green label = down-regulated.